

Photoinduced Dynamics and Toxicity of a Cancer Drug in Proximity of Inorganic Nanoparticles under Visible Light

Siddhi Chaudhuri,^[a] Samim Sardar,^[a] Damayanti Bagchi,^[a] Shreyasi Dutta,^[a]
Sushanta Debnath,^[b] Partha Saha,^[b] Peter Lemmens,^[c] and Samir Kumar Pal^{*,[a]}

Drug sensitization with various inorganic nanoparticles (NPs) has proved to be a promising and an emergent concept in the field of nanomedicine. Rose bengal (RB), a notable photosensitizer, triggers the formation of reactive oxygen species under green-light irradiation, and consequently, it induces cytotoxicity and cell death. In the present study, the effect of photoinduced dynamics of RB upon complexation with semiconductor zinc oxide NPs is explored. To accomplish this, we successfully synthesized nanohybrids of RB with ZnO NPs with a particle size of 24 nm and optically characterized them. The uniform size and integrity of the particles were confirmed by high-resolution transmission electron microscopy. UV/Vis absorption and steady-state fluorescence studies reveal the formation of the nanohybrids. ultrafast picosecond-resolved fluorescence stud-

ies of RB–ZnO nanohybrids demonstrate an efficient electron transfer from the photoexcited drug to the semiconductor NPs. Picosecond-resolved Förster resonance energy transfer from ZnO NPs to RB unravel the proximity of the drug to the semiconductor at the molecular level. The photoinduced ROS formation was monitored using a dichlorofluorescein oxidation assay, which is a conventional oxidative stress indicator. It is observed that the ROS generation under green light illumination is greater at low concentrations of RB–ZnO nanohybrids compared with free RB. Substantial photodynamic activity of the nanohybrids in bacterial and fungal cell lines validated the in vitro toxicity results. Furthermore, the cytotoxic effect of the nanohybrids in HeLa cells, which was monitored by MTT assay, is also noteworthy.

1. Introduction

In the last two decades, there has been phenomenal progress in the field of targeted drug delivery by using nanomaterials to increase solubility, prolong the half-life and diminish the immunogenicity of the drug.^[1–4] Semiconductor nanoparticles (NPs) with their distinct physicochemical properties have several biomedical applications in bioimaging and drug delivery. ZnO NPs, unlike most semiconductor NPs, are less toxic, low cost with reasonable biocompatibility, and hence, are amenable to serve as productive drug-delivery vehicles.^[5,6] ZnO NPs are attributed with exclusive properties, that is, their size is similar to that of biomolecules and they have copious functionalities on large surface areas. Nanohybrids, consisting of drug-loaded ZnO NPs or ZnO hollow spheres incorporating drugs, promote the intracellular delivery of the nanoparticles enabling the in-

vasion of cancer cells through precise ligand–receptor recognition or by nonspecific binding forces, such as hydrophobic and coulombic interactions.^[5] As ZnO NPs possess a wide band gap of 3.3 eV, they can only be excited under UV light with a wavelength of less than 380 nm. It is not judicious to use UV light for in vivo assays, as it has a deep penetration depth and is detrimental to health. Fortuitously, ZnO NPs serve as competent drug-delivery vehicles in photodynamic therapies (PDT), which are effective in obliterating dangerous drug-resistant pathogens when standard antibiotic therapies fail and destroying somatic cells in cancer therapy.^[7] PDT is a nonthermal and minimally invasive technique, which involves the activation of a photosensitizing agent by light ranging from ultraviolet-A (UV-A) to near-infrared wavelengths.^[8] A photosensitizer (PS) absorbs photons and is elevated to a singlet excited state prior to exposure to light of a particular frequency.^[9] The excited state of the photosensitizer either decays back to the ground state or converts into the triplet state, subject to intersystem crossing. The excited triplet state then reacts with ambient oxygen and generates reactive oxygen species (ROS), which are cytotoxic and kill cells by reacting with intracellular components, thereby destructing both cell walls as well as DNA.^[7,10] Generally, photosensitizers possess a high absorption coefficient in the spectral region of the excitation wavelength, pertinent energy in the triplet state, so that effective energy transfer to ground-state oxygen occurs and immense quantum yields of the triplet state. Moreover, they also exhibit long triplet-state lifetimes, as the efficiency of the photosensitizer is de-

[a] S. Chaudhuri, S. Sardar, D. Bagchi, Dr. S. Dutta, Prof. S. K. Pal
Department of Chemical, Biological & Macromolecular Sciences
S. N. Bose National Centre for Basic Sciences
Block JD, Sector III, Salt Lake
Kolkata 700098 (India)
E-mail: skpal@bose.res.in

[b] Dr. S. Debnath, Prof. P. Saha
Crystallography and Molecular Biology Division
Saha Institute of Nuclear Physics
Sector I, Block AF, Bidhannagar
Kolkata 700064 (India)

[c] Prof. P. Lemmens
Institute for Condensed Matter Physics
TU Braunschweig, Mendelssohnstraße 3
38106 Braunschweig (Germany)

pendent on the photophysical properties of its lowest excited triplet state and its favorable photostability.^[11]

Rose bengal (RB; 4,5,6,7-tetrachloro-20,40,50,70-tetraiodo-fluorescein disodium) is a water-soluble, anionic, xanthene photosensitizer, which generates singlet oxygen ($^1\text{O}_2$) from oxygen molecules (O_2) if irradiated with green light.^[12–15] The presence of halogen atoms in RB molecule increases the ability of intersystem crossing to the triplet state, which leads to the generation of singlet oxygen.^[16] Therefore, RB is considered as a propitious sensitizer in PDT of tumors with minimal side effects.^[17–19] In addition, it is commonly used in ophthalmology and has microbiocidal activity against bacteria, viruses, fungi and protozoa.^[20–22] The small penetration depth of green light makes RB particularly useful in treatments of many cutaneous lesions and dermatological diseases.^[23] There are considerable literature reports that describe the use of RB as a photodynamic sensitizer for cancer chemotherapy.^[24] Constructive photosensitization predominantly depends on the physical and chemical characteristics of the PS, such as chemical purity, charge, solubility, distinct localization in tumor cells, sufficiently long residence time, and minimal time interval between the drug administration and its accumulation in neoplastic cells. Moreover, the PS should be easily cleared from normal tissues, undergo excitation at a wavelength with favorable tissue penetration, and show no toxicity in the dark.^[25] The intracellular localization and uptake of a photosensitizer in cells is vital to the photodynamic process as the photoinduced cellular damage occurs proximally with the oxidizing species formed by the excited molecules. The anionic nature and poor lipid solubility of RB obstructs its capability to cross biological membrane barriers, which restricts its clinical application.^[26] There are earlier reports in which the photodynamic efficiency of RB has been improved by using delivery carriers such as liposomes,^[26,27] by developing hydrophobic derivatives (e.g. phosphate or acetate), or by tagging with organically modified Si NPs.^[28–30] In addition, there are studies that report the conjugation of RB with biocompatible polymers and even gold nanorods for potent photodynamic activity.^[31–34] One of our previous articles reports the sensitization of an effective cancer drug, protoporphyrin IX (PP) with ZnO NPs. We subsequently explored the photoinduced ultrafast dynamics of the NP sensitized drug and proved that the nanohybrid displays improved activity in PDT in comparison with that of the free drug. ZnO NPs serve as drug delivery vehicles and assist the charge separation, which in due course enhances the drug activity.^[35] Furthermore, in a complementary study, we sensitized vitamin B₂, a notable antioxidant, with various NPs and modulated the radical scavenging property.^[36]

Despite the importance of the topic and to the best of our knowledge, there is no literature to date that reports the sensitization of RB with ZnO NPs leading to an increase of the photodynamic activity of the drug. Herein, in the present work, we synthesized nanohybrids of RB with ZnO NPs of approximately 24 nm in size. The sizes of the NPs and crystallinity were confirmed using high-resolution transmission electron microscopy (HRTEM). Picosecond-resolved fluorescence experiments on the nanohybrids were performed to understand the efficient elec-

tron transfer from photoexcited RB to ZnO NPs, which eventually upgrades the ROS activity in the RB–ZnO nanohybrids. Picosecond-resolved Förster resonance energy transfer (FRET) from ZnO NPs to RB was used to understand the nanohybrid formation at the molecular level. The ROS formation was monitored by dichlorofluorescein (DCFH) oxidation. Enhanced ROS generation was observed in the presence of the RB–ZnO nanohybrids compared with that of free RB upon green light illumination. The nanohybrid was used as a model photodynamic therapeutic agent in bacterial, fungal, and HeLa cell lines.

2. Results and Discussion

Figure 1a depicts a characteristic HRTEM image of the ZnO NPs. An interplanar distance of approximately 0.25 nm, which corresponds to the spacing between two (002) planes, was determined from the lattice fringe of the ZnO NPs. The average particle size was deduced from our experimental TEM data and found to be approximately 23.9 ± 0.5 nm. The complexation of RB and the ZnO NPs can be understood by using UV/Vis spectroscopy (Figure 1b). The major absorption peak of RB appears at 560 nm with a shoulder at 540 nm in acetonitrile. The characteristic peaks of both RB and ZnO are observed in the nanohybrids. There is a 5 nm peak shift in the absorbance maxima of RB and ZnO in the RB–ZnO nanohybrid, compared with free RB and ZnO NPs, respectively. This observation indicates that there is a perturbation in the molecular structure of RB when bound to the surface of ZnO NPs.^[37] RB loading on ZnO NPs and the thermal stability of the nanohybrids were studied by thermogravimetric analysis (TGA). Figure 1c shows the thermogravimetric curves of RB, ZnO, and RB–ZnO. An onset at about 330 °C and a major decomposition at 400–500 °C for RB are depicted in the TGA plot, whereas pure ZnO NPs are stable, with negligible decomposition in air in the range of 30–600 °C. The thermal decomposition of about 2.5% of the nanohybrids in between 400–500 °C is attributed to the presence of RB molecules. The inset of Figure 1c shows the enlarged graph of RB–ZnO degradation. The number of RB molecules on one ZnO NP was calculated to be 643, which is consistent with the value calculated from the UV/Vis absorption spectra. The absorption spectrum of the RB–ZnO nanohybrids after baseline correction was exploited to quantify the number of RB molecules on a ZnO surface of 30 nm. The RB concentration was calculated from the absorbance maxima at 560 nm, as ZnO has no absorbance above 380 nm.

The emission spectra of RB and RB–ZnO in acetonitrile are shown in Figure 2a and the corresponding excitation spectra are shown in the inset of Figure 2a. RB exhibits an emission peak at 570 nm in acetonitrile upon excitation at 510 nm. RB emission is significantly quenched when it is attached to the ZnO NPs. This observation indicates the efficient nonradiative photoinduced processes from RB to ZnO NPs. To further study the quenching, time-resolved fluorescence transients were carried out. The fluorescence decay profiles for free RB and RB–ZnO were obtained upon excitation at 510 nm in acetonitrile and monitored at 570 nm (Figure 2b). The time constants of the photoluminescence (PL) transients at 570 nm for the sin-

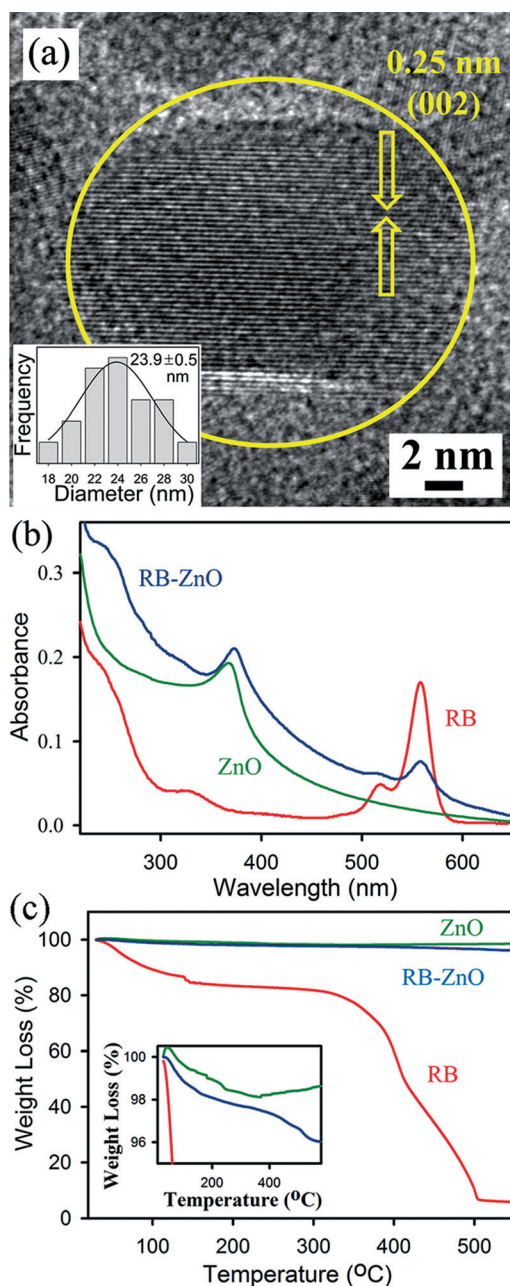


Figure 1. a) HRTEM image of ZnO NPs. Inset: The size distribution of ZnO NPs. b) Absorption spectra of RB-ZnO (blue), RB (red), and ZnO (green). c) TGA profile of RB-ZnO (blue), RB (red), and ZnO (green).

glet excited state of RB in acetonitrile showed single exponential decay, with a lifetime of 2.42 ns. The quenching of the life-

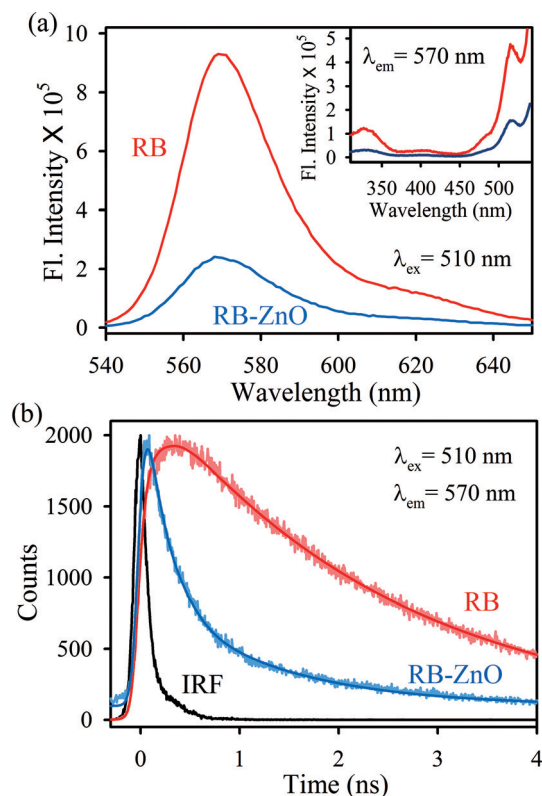


Figure 2. a) Room temperature PL spectra of RB (red) and RB-ZnO (30 nm; blue) upon excitation at 510 nm. Inset: The excitation spectra of RB (red) and RB-ZnO (30 nm; blue) at detection wavelength 570 nm. b) Fluorescence decay profiles of RB (red) and RB-ZnO (30 nm; blue) upon excitation at 510 nm and detection wavelength at 570 nm.

time transients was observed in RB-ZnO with an average lifetime of 0.11 ns after the timescales are fitted by biexponential decay. The fitting parameter details of the fluorescence decays are displayed in Table 1. The average lifetime of the RB in the presence of ZnO NPs is faster owing to efficient electron transfer from excited RB to the conduction band of the ZnO NPs. A RB-ZnO nanohybrid using ZnO NPs with an approximate size of 24 nm, which does not have intrinsic defect state emission, was used to study the interfacial dynamics. The 5 nm-sized ZnO NPs, which have an intrinsic defect state emission, were used to investigate the molecular proximity between RB and ZnO NPs by using the FRET technique.

ZnO NPs have a particle size of 5 nm has a broad steady-state emission in the blue-green region, owing to defect centers located near the surface of the NPs (Figure 3a). The broad

Sample	Excitation wavelength [nm]	Detection wavelength [nm]	τ_1 [ns]	τ_2 [ns]	τ_3 [ns]	τ_{avg} [ns]
RB	510	570	2.42 (100%)	–	–	2.42
RB-ZnO	510	570	0.04 (80%)	0.36 (20%)	–	0.11
ZnO (5 nm)	375	550	0.60 (53%)	13.91 (47%)	–	6.85
RB-ZnO (5 nm)	375	550	0.09 (63%)	0.52 (29%)	7.58 (8%)	0.81

[a] Numbers in the parenthesis indicate relative weighting.

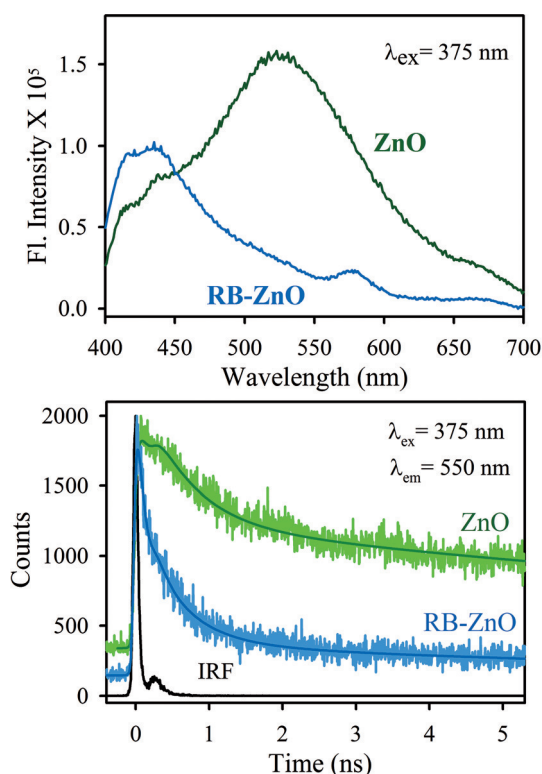


Figure 3. a) Emission spectra of ZnO (5 nm; green) and RB-ZnO (5 nm; blue) upon excitation at 375 nm. Inset: The spectral overlap between ZnO (5 nm) emission and RB absorption spectra. b) Fluorescence decay profiles of ZnO (5 nm; green) and RB-ZnO (5 nm; blue) upon excitation at 375 nm and at a detection wavelength at 550 nm.

emission arises from two different vacancy centers, one as a result of doubly charged vacancy centers (V_o^{++}) located at 555 nm (P_2) and the other arises from singly charged vacancy centers (V_o^+) located at 500 nm (P_1).^[38,39] There was a considerable decrease in the intensity of the defect-state emission of the ZnO NPs in the nanohybrid, which occurs as a consequence of effective nonradiative photoinduced processes from ZnO NPs to the RB. The spectral overlap between the donor ZnO NP emission and the RB absorption (Figure 3 a, inset) indicates the plausibility of convenient energy transfer from ZnO NPs to RB. In this regard, here we propose the phenomenon of FRET from the ZnO NPs (donor) to the RB (acceptor). FRET is a convenient tool to measure the donor-acceptor distance and so it is like a “spectroscopic ruler”.^[40] The fluorescence decay transients of the 5 nm ZnO NPs (donor) in the presence and absence of the RB (acceptor) were measured at 550 nm (P_2 , defect center near the surface) after excitation at 375 nm (Figure 3 b). There was a prominent quenching in the excited-state lifetime of ZnO NPs attached RB in comparison with bare ZnO NPs. The estimated distance between the donor ZnO NPs and the drug is 1.5 nm. The calculated energy transfer is 88% and the overlap integral $[J(\lambda)]$ is $2.98 \times 10^{15} \text{ m}^{-1} \text{ cm}^{-1} \text{ nm}^4$. Thus, the calculated FRET distance confirms the proximity of the RB drugs to the ZnO NPs.

After investigation of the interfacial dynamics and molecular proximity, the rate of ROS production was evaluated by the

conversion of DCFH into dichlorofluorescein (DCF) in an aqueous medium. DCFH is a widely known marker that is used in ROS detection assays.^[41,42] The ROS generated in the medium, oxidized nonfluorescent DCFH into fluorescent DCF. The fluorescence emission intensity of DCF was monitored with respect to time (Figure 4a). There was a maximum enhancement of fluorescence intensity under green-light irradiation in RB-ZnO nanohybrids; ROS production increases almost twofold in RB-ZnO compared with free RB. A control experiment was performed where ZnO NPs upon green-light illumination show negligible ROS generation as the NPs lack photon absorption in the green zone of optical spectrum. However, DCFH oxida-

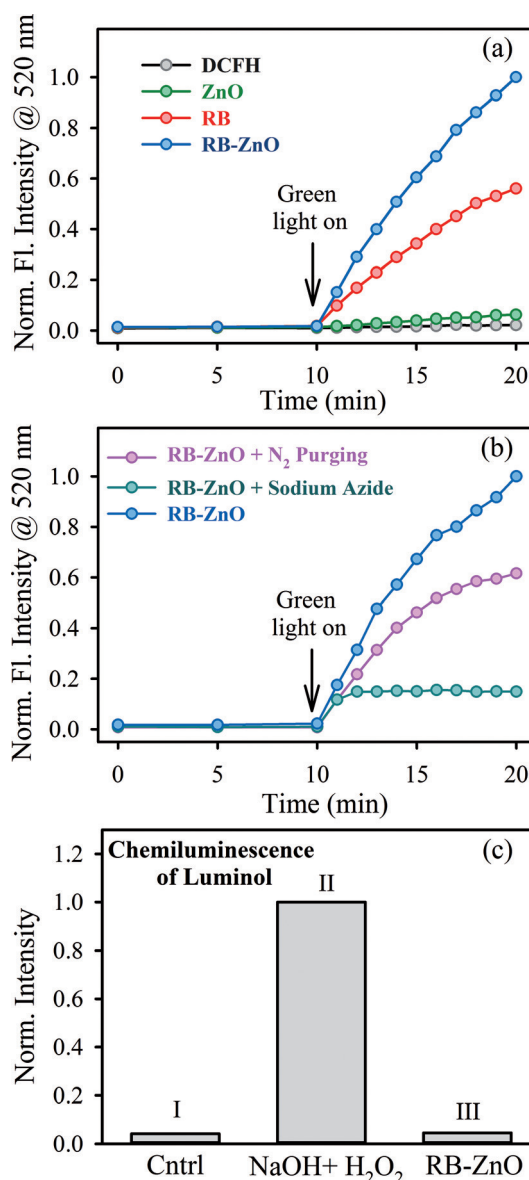


Figure 4. a) DCFH oxidation with respect to time with addition of RB-ZnO (blue), RB (red), ZnO (green), and control DCFH (black) under dark with subsequent green-light irradiation. b) DCFH oxidation with respect to time with RB-ZnO addition in an atmosphere of purged nitrogen (pink), sodium azide (green), and a control (blue) under dark with subsequent green-light irradiation. c) Chemiluminescence of luminol prior to green-light illumination for 15 min for the control (I), NaOH + H_2O_2 (II) and RB-ZnO (III).

tion is inconclusive in determining the nature of generated ROS that is, whether they are singlet oxygen or superoxide anions. On the other hand, Luminol oxidizes to produce chemiluminescence in the presence of superoxide.^[43] It is seen in Figure 4c that no chemiluminescence is obtained in the presence of RB-ZnO after green-light irradiation for 15 min, which rules out the possibility of superoxide generation by the nano-hybrid. To elucidate the involvement of singlet oxygen, the DCFH oxidation assay was performed in the presence of sodium azide, which is a well-known singlet-oxygen quencher.^[44] As shown in Figure 4b, the rate of ROS generation was inhibited in presence of sodium azide. These observations indicate that the nature of ROS is predominantly singlet oxygen rather than superoxide anions, which is consistent with the report of mechanistic pathway of ROS upon photoirradiation of RB alone.^[11] To investigate the role of dissolved oxygen in water, the DCFH oxidation assay was performed after nitrogen purging for one hour. The decrease in DCFH oxidation indicates that the dissolved oxygen in the medium assists in the generation of singlet oxygen. Therefore, when conjugated with RB drugs ZnO NPs, not only aid efficient drug delivery, but also augment ROS formation, due to the enhanced charge separation of the excited drug in the proximity of the semiconductor NPs.

The in-depth characterization studies and analysis of photo-induced dynamics in RB-ZnO nano-hybrid was followed by the use of the nano-hybrid as an efficacious photodynamic therapeutic agent. To confirm the in vitro results of ROS generation in the medium, the RB-ZnO nano-hybrid was employed to inhibit the growth of *Escherichia coli* (*E. coli*) and *Candida albicans* (*C. albicans*). Nano-hybrids contain RB-conjugated ZnO NPs with a particle size of 24 nm rather than 5 nm, due to their lower in vivo toxicity.^[45] The images of *E. coli* cultures treated with RB-ZnO nano-hybrids with and without green light are shown in Figure 5b,c. Bacterial growth inhibition prior to the photodynamic treatment is distinctly observed. The petri plate with RB-ZnO along with green-light exposure contains a significantly less number of colonies. To rule out toxicity that solely arises from the free drug and ZnO NPs, control plates with equimolar concentrations of drug and NPs were included in the experiment. To assess the viability, bacterial colonies were counted for the control along with ones treated with RB drugs, ZnO NPs, and RB-ZnO nano-hybrids with and without green-light exposure (Figure 5a). The colony forming unit (CFU) in the control and ZnO-treated samples are almost similar in the presence and absence of green light. This observation indicates that the concentration of ZnO NPs used in the assay shows minimal toxicity. 30% bacterial growth inhibition is observed in case of RB-treated samples, whereas a maximum inhibition of 65% was deduced for the RB-ZnO treated sample after photodynamic treatment. Similarly, the nano-hybrid has a lethal effect on fungal cells under green light. Figure 6b,c shows pictures of *C. albicans* cultures incubated with RB-ZnO nano-hybrids in the presence and absence of green-light irradiation. There is 26% fungal inhibition in samples treated with RB prior to photodynamic treatment. The fungal inhibition increased to 54% when RB-ZnO is used in

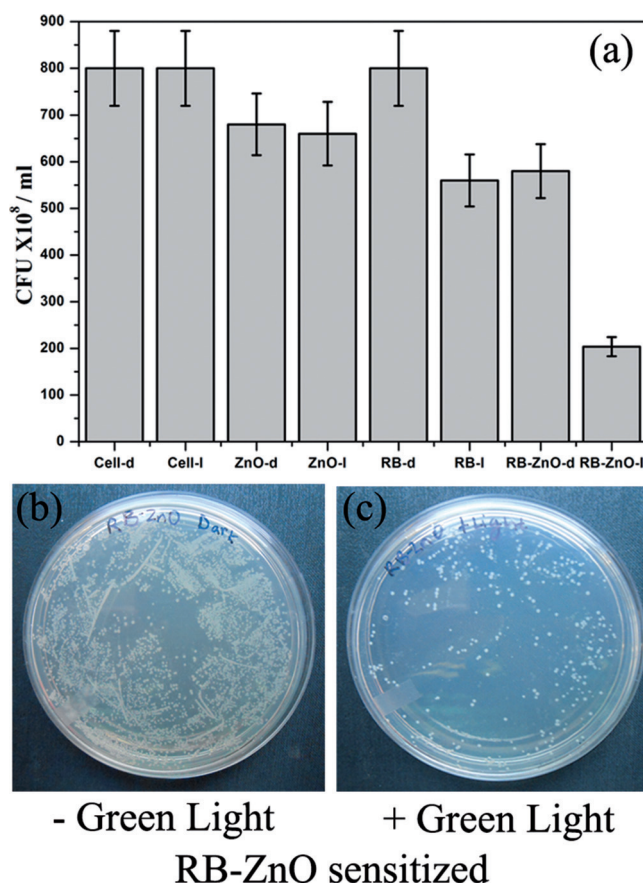


Figure 5. a) Antibacterial activity of RB-ZnO, RB, and ZnO in the presence (with suffix -l) and absence (with suffix -d) of green light. Images of RB-ZnO-treated *E. coli* plates in the absence (b) and presence (c) of green light.

the assay. The antimicrobial results vividly denote the active role of increased ROS formation in the presence of RB-ZnO nano-hybrids compared with that of free RB. The in vitro cytotoxicity assays were conducted in a HeLa cell line using MTT, which is a model marker of cell viability.^[46] Bioreduction of MTT leads to formazan production,^[47] which was estimated at 570 nm. The cell cytotoxicity profile of RB along with the nano-hybrid is illustrated in Figure 7a. The cells were stained with 4',6-diamidino-2-phenylindole (DAPI) before taking the microscopic images of the control and RB-ZnO-treated cells. DAPI specifically stains the chromatin of the nuclei and has a blue emission.^[48] A distinct change in morphology with rounded nucleus is observed for RB-ZnO-treated cells under green-light irradiation (Figure 7e) compared with that in the dark (Figure 7d), whereas the morphology of the control cells remain intact (Figure 7b,c). After seeding 5000 cells per well in a 96-well plate, the cells were subjected to drug treatment with RB, ZnO NPs, and RB-ZnO followed by green-light exposure for four hours. The cells were then incubated overnight at 37 °C in an atmosphere of 5% CO₂ before the MTT assay was performed. The experiment was performed in triplicate and the cell viability was determined by comparison with the control plate. The cell viability for free RB was reduced to half and the value was less than one third when the nano-hybrid was used under green-light irradiation. However, ZnO NPs showed mini-

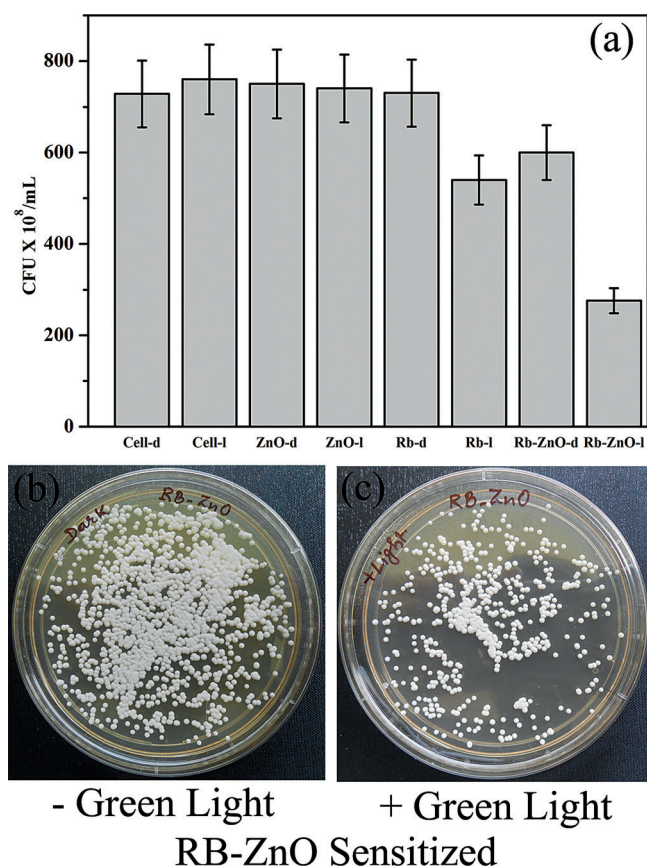


Figure 6. a) Antifungal activity of RB-ZnO, RB, and ZnO in the presence (with suffix -l) and absence (with suffix -d) of green light. Images of RB-ZnO treated *C. albicans* plates in the absence (b) and presence (c) of green light.

mal cell cytotoxicity. The enhanced ROS generation, as a result of charge separation of the drug in the proximity of semiconductor NPs, is responsible for the augmentation of the drug activity. The present study will therefore be helpful for the design efficient photodynamic drugs.

3. Conclusions

The application of RB as a photodynamic therapeutic agent has a long record of pragmatic evidence. In the present study, we illustrated the vital photoinduced dynamics of RB upon complexation with semiconductor ZnO NPs. We synthesized nanohybrids of RB with ZnO NPs of approximately 24 nm in size and characterized them by HRTEM, UV/Vis absorption, and steady-state fluorescence studies. Picosecond-resolved FRET was employed to reveal the proximity of the drug and the semiconductor at the molecular level. It was inferred that the energy is transferred from the defect-state emission of ZnO NPs to RB upon excitation with green light. Furthermore, picosecond-resolved fluorescence studies on RB-ZnO reveal an effective electron migration from photoexcited RB to ZnO NPs, resulting in elevation of the ROS activity in the nanohybrid. The dichlorofluorescein (DCFH-DCF) oxidation assay proved that ROS generation is more than twofold in magnitude greater in the nanohybrid than for the free drug. Moreover, the pho-

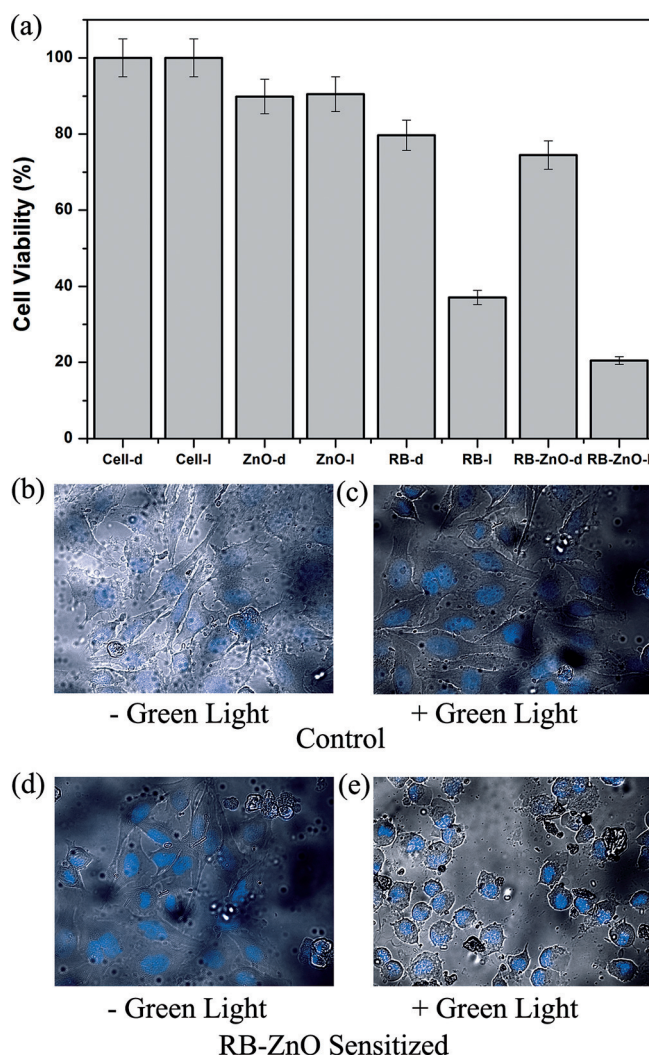


Figure 7. a) In vitro cytotoxicity assay in HeLa cells with RB-ZnO, RB, and ZnO with MTT as an indicator dye in the presence (with suffix -l) and absence (with suffix -d) of green light. Images of control and RB-ZnO treated HeLa cells in the absence (b, d) and the presence (c, e) of green light.

photodynamic activity of the nanohybrid in bacterial, fungal, and HeLa cell lines corroborates the in vitro ROS detection assay. Hence, these studies could be incorporated in the development of safe, beneficial, and low-cost alternative photodynamic therapeutic agents to treat various diseases.

Experimental Section

In this study, the chemicals used for the synthesis were of analytical grade and were used without further purification. ZnO NPs (approximately 30 nm in size) and rose bengal were purchased from Sigma-Aldrich. The suitable solvents were acetonitrile and DMSO (Merck). As an aqueous solution, Millipore water was used.

Synthesis of ZnO NPs and RB Nanohybrids

5 nm ZnO NPs were synthesized using a standard synthesis procedure.^[35] A 0.5 mM RB solution was prepared in acetonitrile.

1 mg mL⁻¹ of 30 nm ZnO NPs were added to the prepared the RB solution and the mixture was stirred for 12 h. ZnO NP sensitization with the RB dye was carried out at room temperature and under dark conditions. The solution was centrifuged for 30 minutes and the clear supernatant solution of free dyes was decanted after the sensitization process. The samples were dried over a water bath after washing 3–4 times with acetonitrile.

Characterization Methods

A dilute drop of the ZnO samples was cast onto carbon-coated copper grids for the TEM experiments. At a magnification of 100000x, the particle sizes were determined from micrographs using an FEI (Technai S-Twin, operating at 200 kV) instrument. TGA of RB, ZnO NPs, and RB–ZnO were performed under a nitrogen atmosphere. The samples were heated from 30 to 600 °C at a rate of 10 °C min⁻¹ by using a PerkinElmer TGA-50H. For the optical studies, the steady-state absorption and emission were detected with a Shimadzu spectrophotometer (UV-2600) and a Horiba fluorolog, respectively. Time-resolved emission measurements were carried out using a time-correlated single-photon counting (TCSPC) setup^[49] from Edinburgh Instruments (instrument response function, IRF_e = 80 ps, excitation at 375 and 510 nm). A nonlinear least-square fitting procedure was used to fit the observed fluorescence transients, as reported in our previous publications.^[50,51]

FRET Calculations

The consecutive procedure was used to deduce the FRET efficiency^[35,52,53] of the donor (ZnO) and then the donor–acceptor distance. R_0 is the Förster distance which is given by Equation (1):

$$R_0 = 0.211 \times [\kappa^2 n^{-4} Q_D J^6]^{1/6} \text{ (in } \text{Å}) \quad (1)$$

where κ^2 is a factor that describes the relative space orientation of the transition dipoles of the donor and acceptor and the value of κ^2 is approximated to be 2/3 as the donor and acceptor randomize by rotational diffusion before energy transfer. The refractive index (n) of the medium was found to be 1.47. Q_D , the integrated quantum yield of the donor in the absence of acceptor, was measured to be 3.8×10^{-3} . J , the overlap integral, which depicts the degree of spectral overlap between the donor emission and the acceptor absorption, is given by Equation (2):

$$J(\lambda) = \frac{\int_0^\infty F_D(\lambda) \epsilon_A(\lambda) \lambda^4 d\lambda}{\int_0^\infty F_D(\lambda) d\lambda} \quad (2)$$

where, $F_D(\lambda)$ is the fluorescence intensity of the donor in the wavelength range of λ to $\lambda + d\lambda$ and is dimensionless. $\epsilon_A(\lambda)$ is the extinction coefficient (in M⁻¹ cm⁻¹) of the acceptor at λ . If λ is in nm, then J is in units of M⁻¹ cm⁻¹ nm⁴. The donor–acceptor distance (r_{DA}) is estimated by using Equation (3):

$$r_{DA}^6 = \frac{[R_0^6(1 - E)]}{E} \quad (3)$$

Here E is the efficiency of energy transfer. The transfer efficiency is derived using the relative fluorescence lifetime of the donor, in the absence (τ_D) and the presence (τ_{DA}) of the acceptor [Eq. (4)]:

$$E = 1 - \frac{\tau_{DA}}{\tau_D} \quad (4)$$

From the average lifetime calculation for the RB–ZnO nanohybrids, we attained the donor–acceptor distance (r_{DA}) by combining Equations (3) and (4) [Eq. (5)]:

$$r^6 = [R_0^6(1 - E)]/E \quad (5)$$

Preparation of Dichlorofluorescein (DCFH) and ROS Measurements

DCFH was synthesized from DCFH–DA (dichlorofluorescein diacetate; Calbiochem). 1.0 mM DCFH–DA in methanol (0.5 mL) was mixed with 0.01 N NaOH (2.0 mL) at room temperature for 30 min. 25 mM NaH₂PO₄ (10 mL) was used to neutralize the mixture. The measurements were conducted in a total volume of 2.0 mL of water, which contained DCFH solution (10 μL), RB (3 μM), ZnO (200 μM), and RB–ZnO (individual concentrations of RB and ZnO in the nanohybrid in DMSO are 3 and 200 μM, respectively).

Bacterial Strain and Culture Conditions

The antibacterial assay was performed using *E. coli* XL1-Blue cells. The cells were cultured at 37 °C in a liquid LB (Luria–Bertani) medium. When the optical density reached around 0.6, the culture was serially diluted ten thousand times with the LB medium and treated with drugs containing RB (3 μM), ZnO (200 μM), and RB–ZnO (individual concentrations of RB and ZnO in the nanohybrid in DMSO are 3 and 200 μM respectively). The RB concentration was calculated from the absorption maxima around 540 nm, as ZnO does not absorb above 380 nm. The samples were then kept under the green light (λ_{max} of 520 nm, ≈ 14600 LUX) for 4 h. The photodynamic effect was studied by placing the treated samples in LB agar plates and incubating them overnight at 37 °C. After incubation overnight, the colonies were counted.

Fungal Strain and Culture Conditions

The antifungal assay was studied using *C. albicans*. The cells were cultured at 30 °C in a liquid yeast extract peptone dextrose (YEPD) broth. When the optical density reached around 0.6, the inoculum was serially diluted ten thousand times with the YEPD medium and treated with RB (3 μM), ZnO (200 μM), and RB–ZnO (individual concentrations of RB and ZnO in the nanohybrid in DMSO were 3 and 200 μM respectively). The samples were then exposed to green light (λ_{max} of 520 nm, ≈ 14600 LUX). To study the effect of light, the inoculum was plated and incubated for 24 h. Finally, the colonies were counted after the incubation.

MTT Assay

HELA cells were grown in Dulbecco's modified eagle's medium (DMEM; HiMedia) supplemented with 10% fetal bovine serum (FBS; Gibco) and 1.0% penicillin/streptomycin (HiMedia) and cultured at 37 °C, 5.0% CO₂, and 100% humidity. 1.9×10^5 cells were seeded and cultured in 10% FBS-supplemented DMEM. Cells (165 μL) from the stock culture were seeded in a 96-well plate for the photodynamic treatment. Cells were incubated with RB (3 μM), ZnO (200 μM), and RB–ZnO (individual concentration of RB and ZnO in the nanohybrid in DMSO were 3 and 200 μM, respectively) for 1 h and were exposed to the green light (λ_{max} : 520 nm, ≈ 14600

LUX) for 4 h. After overnight incubation, the MTT assay was performed with fresh DMEM medium. 5 mg mL⁻¹ MTT stock was prepared in sterile PBS. 15 µL of the MTT stock solution was added to the cells and incubated for 4 h. DMSO (150 µL) was added to solubilize the formazan before taking the absorbance at 570 nm.

Fluorescence Microscopy Studies

Micrographs of HeLa cells were taken using Zeiss AxioObserver Z1 Fluorescence Microscope, which was attached with an Apotome apparatus. The cells were washed twice with PBS and fixed with 4% paraformaldehyde (Sigma) according to the standard protocol.^[54] Finally, they were stained with Fluoroshield mounting medium with DAPI (ABCAM) before capturing the images at 40x magnification.

Acknowledgements

S.C. thanks Council of Scientific and Industrial Research (CSIR, India) for providing the research fellowship. We would like to thank the Department of Science and Technology (DST, India) (DST-TM-SERI-2k11-103 and SB-S1-PC-011-2013) and Department of Atomic Energy (DAE, India) (2013-37P-73-BRNS) for financial grants. P.L. acknowledges the NTH-School "Contacts in Nanosystems" and the Braunschweig International Graduate School of Metrology.

Keywords: drug delivery · photochemistry · FRET · nanoparticles · reactive oxygen species (ROS)

- [1] J. B. Hall, M. A. Dobrovolskaia, A. K. Patri, S. E. McNeil, *Nanomedicine* **2007**, *2*, 789–803.
- [2] J. Lenard, A. Rabson, R. Vanderloef, *Proc. Natl. Acad. Sci. USA* **1993**, *90*, 158–162.
- [3] T. S. Hauck, S. Giri, Y. Gao, W. C. Chan, *Adv. Drug Delivery Rev.* **2010**, *62*, 438–448.
- [4] V. B. Arce, S. G. Bertolotti, F. J. Oliveira, C. Airoidi, A. Arques, L. Santos-Juanes, M. C. Gonzalez, C. J. Cobos, P. E. Allegretti, D. O. Mártire, *Photochem. Photobiol. Sci.* **2012**, *11*, 1032–1040.
- [5] H.-M. Xiong, *Adv. Mater.* **2013**, *25*, 5329–5335.
- [6] J. W. Rasmussen, E. Martinez, P. Louka, D. G. Wingett, *Expert Opin. Drug Delivery* **2010**, *7*, 1063–1077.
- [7] H. Kitching, A. J. Kenyon, I. P. Parkin, *Phys. Chem. Chem. Phys.* **2014**, *16*, 6050–6059.
- [8] J. Moan, Q. Peng, *Anticancer Res.* **2003**, *23*, 3591–3600.
- [9] B. Q. Spring, I. Rizvi, N. Xu, T. Hasan, *Photochem. Photobiol. Sci.* **2015**, *14*, 1476–1491.
- [10] X. Ragàs, L. P. Cooper, J. H. White, S. Nonell, C. Flors, *ChemPhysChem* **2011**, *12*, 161–165.
- [11] M. C. DeRosa, R. J. Crutchley, *Coord. Chem. Rev.* **2002**, *233*, 351–371.
- [12] S. D.-M. Islam, O. Ito, *J. Photochem. Photobiol. A* **1999**, *123*, 53–59.
- [13] S. H. Mousavi, J. Tavakkol-Afshari, A. Brook, I. Jafari-Anarkooli, *Food Chem. Toxicol.* **2009**, *47*, 855–859.
- [14] E. Panzarini, V. Inguscio, G. M. Fimia, L. Dini, *PLoS One* **2014**, *9*, e105778.
- [15] C. R. Lambert, I. E. Kochevar, *Photochem. Photobiol.* **1997**, *66*, 15–25.
- [16] F. F. Sperandio, Y. Y. Huang, M. R. Hamblin, *Recent Pat. Anti-Cancer Drug Discovery* **2013**, *8*, 108–120.
- [17] E. Panzarini, V. Inguscio, L. Dini, *Cell Death Dis.* **2011**, *2*, e169.
- [18] S. S. Mohideen, Y. Yamasaki, Y. Omata, L. Tsuda, Y. Yoshiike, *Sci. Rep.* **2015**, DOI: 10.1038/srep10821.
- [19] L. Dini, V. Inguscio, B. Tenuzzo, E. Panzarini, *Cancer Biol. Ther.* **2010**, *10*, 1048–1055.
- [20] A. C. B. P. Costa, V. M. C. Rasteiro, C. A. Pereira, R. D. Rossoni, J. C. Junqueira, A. O. C. Jorge, *Mycoses* **2012**, *55*, 56–63.
- [21] C. O. Morton, M. Chau, C. Stack, *BMC Microbiol.* **2014**, *14*, 261.
- [22] A. Arboleda, D. Miller, F. Cabot, M. Taneja, M. C. Aguilar, K. Alawa, G. Amescua, S. H. Yoo, J.-M. Parel, *Am. J. Ophthalmol.* **2014**, *158*, 64–70.
- [23] E. Panzarini, V. Inguscio, L. Dini, *Int. J. Photoenergy* **2011**, *2011*, 1–11.
- [24] M. Bolean, P. Paulino Tde, G. Thedei Jr., P. Ciancaglini, *Photomed. Laser Surg.* **2010**, *28*, S79–S84.
- [25] B. J. Park, K.-H. Choi, K. C. Nam, A. Ali, J. E. Min, H. Son, H. S. Uhm, H.-J. Kim, J.-S. Jung, E. H. Choi, *J. Biomed. Nanotechnol.* **2015**, *11*, 226–235.
- [26] C.-C. Chang, Y.-T. Yang, J.-C. Yang, H.-D. Wu, T. Tsai, *Dyes Pigm.* **2008**, *79*, 170–175.
- [27] M. Fadel, K. Kassab, *Trop. J. Pharm. Res.* **2011**, *10*, 289–297.
- [28] M. Bottone, C. Soldani, A. Frascini, C. Alpini, A. Croce, G. Bottiroli, C. Pellicciari, *Histochem. Cell Biol.* **2007**, *127*, 263–271.
- [29] A. Uppal, B. Jain, P. K. Gupta, K. Das, *Photochem. Photobiol.* **2011**, *87*, 1146–1151.
- [30] P. K. Gupta, K. Das, M. Sharma, *Procedia Engineering* **2014**, *92*, 9–18.
- [31] A. Shrestha, M. R. Hamblin, A. Kishen, *Antimicrob. Agents Chemother.* **2012**, *56*, 4876–4884.
- [32] M. J. Simpson, H. Poblete, M. Griffith, E. I. Alarcon, J. C. Scaiano, *Photochem. Photobiol.* **2013**, *89*, 1433–1441.
- [33] A. Shrestha, M. R. Hamblin, A. Kishen, *Nanomedicine* **2014**, *10*, 491–501.
- [34] B. Wang, J. H. Wang, Q. Liu, H. Huang, M. Chen, K. Li, C. Li, X. F. Yu, P. K. Chu, *Biomaterials* **2014**, *35*, 1954–1966.
- [35] S. Sardar, S. Chaudhuri, P. Kar, S. Sarkar, P. Lemmens, S. K. Pal, *Phys. Chem. Chem. Phys.* **2015**, *17*, 166–177.
- [36] S. Chaudhuri, S. Sardar, D. Bagchi, S. S. Singha, P. Lemmens, S. K. Pal, *J. Phys. Chem. A* **2015**, *119*, 4162–4169.
- [37] D. Xu, D. C. Neckers, *J. Photochem. Photobiol. A* **1987**, *40*, 361–370.
- [38] A. van Dijken, E. A. Meulenkamp, D. Vanmaekelbergh, A. Meijerink, *J. Phys. Chem. B* **2000**, *104*, 1715–1723.
- [39] K. Vanheusden, W. L. Warren, C. H. Seager, D. R. Tallant, J. A. Voigt, B. E. Gnade, *J. Appl. Phys.* **1996**, *79*, 7983–7990.
- [40] C. J. Breshike, R. A. Riskowski, G. F. Strouse, *J. Phys. Chem. C* **2013**, *117*, 23942–23949.
- [41] S. B. Koevary, *Int. J. Physiol. Pathophysiol. Pharmacol.* **2012**, *4*, 99–107.
- [42] C. P. LeBel, H. Ischiropoulos, S. C. Bondy, *Chem. Res. Toxicol.* **1992**, *5*, 227–231.
- [43] M. M. Tarpey, I. Fridovich, *Circ. Res.* **2001**, *89*, 224–236.
- [44] R. Huang, E. Choe, D. B. Min, *J. Food Sci.* **2004**, *69*, C726–C732.
- [45] S. Nair, A. Sasidharan, V. V. Divya Rani, D. Menon, S. Nair, K. Manzoor, S. Raina, *J. Mater. Sci. Mater. Med.* **2009**, *20*, 235–241.
- [46] K. Chiba, K. Kawakami, K. Tohyama, *Toxicol. in Vitro* **1998**, *12*, 251–258.
- [47] M. Ishiyama, H. Tominaga, M. Shiga, K. Sasamoto, Y. Ohkura, K. Ueno, *Biol. Pharm. Bull.* **1996**, *19*, 1518–1520.
- [48] K. Jin, X. Wang, L. Xie, X. O. Mao, W. Zhu, Y. Wang, J. Shen, Y. Mao, S. Banwait, D. A. Greenberg, *Proc. Natl. Acad. Sci. USA* **2006**, *103*, 13198–13202.
- [49] N. Polley, S. Saha, A. Adhikari, S. Banerjee, S. Darbar, S. Das, S. K. Pal, *Nanomedicine* **2015**, *10*, 2349–2363.
- [50] S. Chaudhuri, S. Batabyal, N. Polley, S. K. Pal, *J. Phys. Chem. A* **2014**, *118*, 3934–3943.
- [51] S. Sardar, S. Sarkar, M. T. Z. Myint, S. Al-Harathi, J. Dutta, S. K. Pal, *Phys. Chem. Chem. Phys.* **2013**, *15*, 18562–18570.
- [52] J. R. Lakowicz, *Kluwer Academic/Plenum*, New York **2006**.
- [53] S. Sardar, P. Kar, S. Sarkar, P. Lemmens, S. K. Pal, *Sol. Energy Mater. Sol. Cells* **2015**, *134*, 400–406.
- [54] E. Harlow, D. Lane, *Cold Spring Harbor Protoc.* **2006**, DOI: 10.1101/pdb.prot4294.

Manuscript received: October 12, 2015

Revised: November 6, 2015

Accepted Article published: November 13, 2015

Final Article published: November 26, 2015